Journal of Magnetic Resonance **155,** 29–38 (2002)
doi:10.1006/jmre.2001.2496, available online at http://www.idealibrary.com on IDEAL®

Cross-Correlation Effects Involving Curie Spin Relaxation in Methyl Groups

P. K. Madhu,[1] Pravat K. Mandal,[2] and Norbert Müller[3]

Institut für Chemie, Johannes Kepler Universität, Altenbergerstrasse 69, A-4040 Linz, Austria

Received June 18, 2001; revised October 18, 2001; published online February 8, 2002

Cross-correlation effects arising in methyl protons due to the simultaneous presence of dipole–dipole, chemical shift anisotropy, and Curie spin relaxation mechanisms in paramagnetic systems are analyzed. We assess the potential of obtaining structural constraints from the cross-correlation of Curie spin relaxation with dipolar relaxation mechanisms among methyl proton spins. By theoretical analysis and numerical simulations we characterize the transfer functions describing the interconversion processes of different ranks of multispin order. The time dependence of these processes contains a new type of structural information, the orientation of the methyl C_3-axis with respect to the electron center. Experimental confirmation is found for selected methyl groups in low spin Fe^{3+} sperm whale myoglobin. © 2002 Elsevier Science (USA)

1. INTRODUCTION

Cross-correlation phenomena due to the simultaneous presence of different nuclear magnetic relaxation mechanisms of the same tensorial rank have been well known since the studies of Shimizu (*1*) and Blicharski (*2, 3*). Cross-correlation terms among chemical shift anisotropy (CSA), dipole–dipole interactions (DD), and quadrupolar interactions have been thoroughly investigated in theory and by experiments (*4–7*). In a weakly coupled spin system the presence of such interference terms causes the creation of longitudinal multispin orders, like two $(2I_{1z}I_{2z})$-, three $(4I_{1z}I_{2z}I_{3z})$-spin order terms by longitudinal relaxation (*4*). Evolution of these multispin orders, which affect both T_1 and NOE measurements, can be monitored in multiple-quantum-filtered experiments (*8–10*). In the case of transverse relaxation the effect of these cross-terms is differential relaxation and consequentially differential broadening of the multiplet components (*11–13*). Interference effects involving an additional relaxation mechanism, Curie spin relaxation (CSR), arising due to the presence of unpaired electron spins (*14, 15*) in paramagnetic systems has been the subject of recent investigations (*16–18*). Although dipolar in character, cross-correlation terms of CSR with internuclear dipolar relaxation mechanism leads to creation of two-spin order, since the spin part of CSR is analogous to that of CSA (*19*). Cross-correlation effects in general and that involving CSR in particular become more significant at higher magnetic fields.

Despite the fact that paramagnetic relaxation of nuclear spins has been the subject of a large number of NMR studies since 1950, many of its facets are gaining renewed importance currently. Following the seminal work of Solomon (*20*) and Solomon and Bloembergen (*21*), the role of CSR was highlighted by Gueron (*14*) and Vega and Fiat (*15*). Cross-correlation effects of CSR can give rise to substantial relaxation-allowed coherence transfer (RACT) peaks as was shown by Bertini *et al.* (*16*) and Qin *et al.* (*17*). The effects of the interference terms involving CSR in various motional regimes have been described in recent works where direct bearing of CSR on structure elucidation has been envisioned (*18, 22–24*).

Recently, substantial interest in cross-correlation phenomena has been generated with the finding that they can be exploited to arrive at structural constraints (*25–27*). This approach can be adapted to paramagnetic systems as CSR cross-terms carry both distance and angular information, the latter being a new type of structural constraint for methyl groups. Such structural refinements can contribute substantially to studies of paramagnetic samples which are otherwise impeded by line broadening due to the fast relaxation of the nuclei in the presence of an unpaired electron center.

In a previous paper we have pointed out the significance of CSR in giving rise to characteristic relaxation patterns of methyl groups in a paramagnetic protein, namely, horse radish peroxidase (HRP), which is probably the first observation of CSR cross-correlation effects involving methyl groups (*28*). Here we analyze the relaxation of methyl groups in the presence of a paramagnetic center, expand the observations and conclusions presented in the previous article (*28*), and propose new applications for molecular geometry refinement. Following the theoretical treatment of the CSR phenomenon in methyl protons, we will show how its cross-correlation with the DD mechanism can lead to useful orientational constraints for methyl groups with a C_3-axis orientation in paramagnetic molecules.

[1] Present address: Department of Chemistry, University of Southampton, Southampton SO17 1BJ, United Kingdom.

[2] Present address: Department of Anesthesiology and Critical Care Medicine, University of Pittsburgh, 3550 Terrace Street, Pittsburgh, PA 15261.

[3] To whom correspondence should be addressed. E-mail: norbert.mueller@jk.uni-linz.ac.at.

1090-7807/02 $35.00

We start by discussing different mechanisms of paramagnetic nuclear relaxation, the electron-nucleus hyperfine and the susceptibility contributions, their relative strengths in influencing both longitudinal and transverse relaxation of protons, the interference effects of CSR with internuclear dipolar relaxation mechanism, and the characteristic spectral signatures and information content of such interference terms. In the discussion we will make use of transfer functions derived from the Redfield matrix to describe the interconversion of coherences and populations as in previous papers (*28–30*). Experiments on myoglobin are then compared with numerical simulations of the transfer functions. Finally, it will be shown that determining the transfer functions allows one to derive novel structural constraints for methyl groups in paramagnetic compounds.

2. PARAMAGNETIC RELAXATION

Nuclear relaxation in the presence of an unpaired electron center is enhanced by the electron-nucleus hyperfine interaction (*31, 32*) and the susceptibility contribution (*14, 15*). The susceptibility contribution is due to the dipolar coupling between the nuclear spins and the thermally averaged electronic spin polarization. The latter being already an average is hence not modulated by the self-relaxation of the electron spin, but only by the reorientational tumbling motion of the molecule and exchange processes. This contribution gives rise to Curie spin relaxation. The CSR mechanism arises via the reorientation of the $\vec{r}$ connecting the nuclear I and the electronic S_e spins, similar to the way the DD mechanism acts between two nuclear spins. Hence the CSR term is modulated by the same molecular tumbling that modulates internuclear dipolar interaction attached to a rigid molecular frame and thus cross-correlation can exist between CSR and dipolar interactions among nuclear spins. Following the definitions of Vega and Fiat (*15*), we designate the dipolar contribution arising between nuclear and electron spins as D_S (S-contribution) and the CSR term as D_χ (χ-contribution). Both D_S and D_χ depend on the distance between the concerned nuclear and electron spins while the Fermi contact term—characterized by the isotropic scalar coupling constant, A—does not. In the following discussion we assume the g tensor to be isotropic of magnitude 2. Sternlicht (*33*) and, more recently, Vasavada and Rao (*34*) and Bertini *et al*. (*35*) have discussed the implications of an anisotropic g tensor and given the expression for the nuclear longitudinal and transverse relaxation times for a general case. The deviations caused by the simplifications are smaller than the experimental error.

In the presence of a paramagnetic center the nuclear Hamiltonian for spin I takes the form

$$\hbar\mathcal{H}_I = \omega_0 I_z + \mathcal{H}^{DD} + \mathcal{H}^{CSA} + \mathcal{H}^{CSR} + KI \cdot (D_S) \cdot S_e + AI \cdot S_e, \quad [1]$$

where I and S_e correspond to the nuclear and the electronic spins, respectively, A is the isotropic scalar coupling constant; and D_S is the dipolar tensor which is traceless. $\mathcal{H}^{DD}$, $\mathcal{H}^{CSA}$, and $\mathcal{H}^{CSR}$, respectively, represent the Hamiltonians corresponding to dipolar interactions between nuclear spins, the CSA interaction of the nuclear spin, and the CSR due to the electron center. Since the role of the last two terms in Eq. [1] is mainly to enhance the nuclear relaxation rates, they can be treated as random field terms for all practical purposes following the definition of Vold and Vold (*36*). Hence, they will not have any cross-correlation term with the other interactions, unless one is dealing with very small molecules. In the following treatment, the spectral densities corresponding to these are added to the diagonal elements of the Redfield relaxation matrix (*37*). K is a constant given by

$$K = \frac{\mu_0}{4\pi}\frac{\gamma\beta_m g}{r^3}, \quad [2]$$

where γ is the gyromagnetic ratio of the protons, β_m is the Bohr magneton, and r is the distance between the centroid of the unpaired electron center and the proton.

Cross-correlation terms exist among CSR, a rank 2 tensor, and DD and CSA, which carry potentially useful structural information. The relaxation enhancement from the hyperfine term has been used successfully, albeit in a qualitative way, for insights into solvent exposure and bleaching of the surface residues of proteins (*38*). It may be also mentioned here that the contribution from the last term in Eq. [1] has proved to be of significance only in cases of hindered methyl rotation as the scalar interaction can get modulated by intramolecular rotation as in the case of methyl groups (*15*). Hence we do not take this term into consideration in the simulations.

Since we are interested in multispin orders the system of methyl protons is treated here as previously (*30*) as a quadrupolar group of spin $F = \frac{3}{2}$ in the symmetry-adapted base shown in Fig. 1 (*30*). The Hamiltonian considered here for the purpose of calculation where we treat only the CSR part of the paramagnetic relaxation (as the hyperfine term contributes only to autocorrelation) is given by (*19, 39, 40*)

$$\hbar\mathcal{H}(t) = \sum_{i<j}\mathcal{H}_{ij}^{DD} + \mathcal{H}_i^{CSA} + \mathcal{H}_{ie}^{CSR}, \quad [3]$$

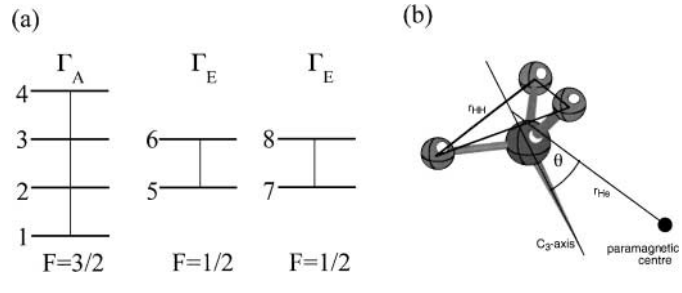

FIG. 1. (a) Symmetry-adapted energy level diagram of a system of three equivalent spins $\frac{1}{2}$ corresponding to a CH_3 group. The energy levels of the three methyl protons are a superposition of one $F = \frac{3}{2}$ and two $F = \frac{1}{2}$ spin subsystems. (b) A schematic of the configuration of the methyl group indicating the geometrical parameters, r_{He} and θ, involved.

where $\mathcal{H}^{DD}$, $\mathcal{H}^{CSA}$, and $\mathcal{H}^{CSR}$, respectively, denote the dipolar, CSA, and CSR Hamiltonians. The indices i and j stand for the nuclear spins and e for the electron spin. We give explicit expressions for only those terms pertaining to CSR. Formulae for CSA and DD interactions may be found in Refs. (*19, 30*). The CSR Hamiltonian may be written as

$$\mathcal{H}_{ie}^{CSR} = \zeta_{ie}^{CSR} \sum_{k=-2}^{2} (-)^k Y_2^{-k}\left(\theta_{ie}^{CSR}(t)\phi_{ie}^{CSR}(t)\right) V_{CSR}^{(k)}(I^i S_e), \quad [4]$$

where I^i and I^j represent nuclear spins, S_e the unpaired electron spin, Y_2^{-k} the second-order spherical harmonics, $\theta_{ij}(t)$ and $\phi_{ij}(t)$ the time-dependent polar coordinates denoting the orientation of the principal axis of the shift tensor with respect to the lab frame, and $V^{(k)}$ the irreducible spin tensors for the DD, $V_{DD}^{(i)}$, CSA, $V_{CSA}^{(i)}$ (*30, 40*) and CSR, $V_{CSR}^{(i)}$ (*19*) ($i = 1, 2, 3$). $V_{CSR}^{(i)}$ may be written in terms of Cartesian (I_z) and shift operators (I_+ and I_-) as

$$\begin{aligned} V_{CSR}^{(0)} &= V_{CSA}^{(0)} = \sqrt{\frac{8}{15}} I_z \\ V_{CSR}^{(\pm 1)} &= V_{CSA}^{(\pm 1)} = \mp \frac{1}{\sqrt{5}} I_{\pm} \\ V_{CSR}^{(\pm 2)} &= V_{CSA}^{(\pm 2)} = 0. \end{aligned} \quad [5]$$

The pre-factor ζ_{ie}^{CSR} is given by

$$\zeta_{ie}^{CSR} = \sqrt{\frac{24\pi}{5}} \hbar \gamma_i \gamma_e. \quad [6]$$

Notice the identical form of the irreducible spin tensors for CSA and CSR. This means that for all computational purposes CSR behaves like CSA although the former is a pairwise dipolar and the latter is a single spin interaction. The consequence of this is the absence of zero- and double-quantum terms for CSR, unlike the internuclear DD interaction. This identical form has been arrived at by shifting the constant coefficients to the spatial part multiplying the spectral densities, which for each of the interactions considered here are given by the usual convention

$$J_r(\omega) = \rho_r \frac{\tau_c}{1 + (\omega\tau_c)^2}, \quad [7]$$

where r stands for DD, CSA, or CSR; ω is the Larmor frequency of the protons; and τ_c is the correlation time assuming isotropic tumbling of a rigid molecule. The constant coefficient ρ_{CSR} can be expressed as (*16*)

$$\rho_{CSR} = \frac{9}{4}\left(\frac{\mu_0}{4\pi}\right)^2 \gamma_H^2 r_{He}^{-6} \hbar^2 \left(\frac{g_e \beta_m \gamma_e B_0 S_e(S_e+1)}{3kT}\right)^2. \quad [8]$$

Both the transverse and the longitudinal nuclear relaxation enhancement due to the electronic relaxation (those due to the S contribution) is added explicitly to the diagonal elements of the Redfield matrix, the spectral densities for which take the form

$$\begin{aligned} J_e^{long}(\omega) &= \frac{2}{3}\left(\frac{A}{\hbar}\right)^2 S_e(S_e+1)\left(\frac{\tau_2}{1+(\omega_e-\omega_I)^2\tau_2^2}\right) \\ &\quad + \frac{2}{15}K_e^2\left(\frac{3\tau_1}{1+(\omega\tau_1)^2} + \frac{7\tau_2}{1+(\omega_e\tau_2)^2}\right) \\ J_e^{tran}(\omega) &= \frac{1}{15}K_e^2\left(4\tau_1 + \frac{3\tau_1}{1+(\omega\tau_1)^2} + \frac{13\tau_2}{1+(\omega_e\tau_2)^2}\right), \end{aligned} \quad [9]$$

where $K_e^2 = K^2 S_e(S_e+1)$. In the above τ_1 and τ_2 are given by

$$\begin{aligned} \frac{1}{\tau_1} &= \frac{1}{\tau_c} + \frac{1}{\tau_M} + \frac{1}{T_{1e}} \\ \frac{1}{\tau_2} &= \frac{1}{\tau_c} + \frac{1}{\tau_M} + \frac{1}{T_{2e}}, \end{aligned} \quad [10]$$

where T_{1e} and T_{2e} are respectively the electronic longitudinal and transverse relaxation times, τ_c is the rotational correlation time for the electron, and τ_M is the residence time of the nucleus when chemical exchange needs to be considered. For the current discussion we neglect τ_M and τ_c since, for the case considered here, the electronic relaxation time is much smaller than the rotational correlation time. Although a few studies have assumed $T_{1e} = T_{2e}$, in general, $T_{2e} < T_{1e}$. We therefore drop the second and third terms in the parantheses of Eq. [9] since $\omega_e = \gamma_e B_0 = 658\omega_H = 658_{\gamma H} B_0$, where ω_e is the Larmor frequency of the electron. Moreover it may be noted that $\omega\tau_1 \ll 1$ but we still retain the form of that spectral density so that its presence at the single-quantum frequency for longitudinal relaxation enhancement and both zero- and single-quantum frequency for transverse relaxation enhancement is clearly shown. The spectral densities for the paramagnetic relaxation enhancement then take the form

$$\begin{aligned} J_e^{long}(\omega) &\approx \frac{2}{15}K_e^2\left(\frac{3T_{1e}}{1+(\omega T_{1e})^2}\right) \\ J_e^{tran}(\omega) &\approx \frac{1}{15}K_e^2\left(4T_{1e} + \frac{3T_{1e}}{1+(\omega T_{1e})^2}\right). \end{aligned} \quad [11]$$

As stated above these are added to the respective diagonal elements of the Redfield matrix. The cross-correlation spectral density is given by

$$J_{kl}(\omega) = P_2\cos(\theta)\sqrt{J_k(\omega)J_l(\omega)}, \quad [12]$$

where $P_2\cos(\theta)$ is the well-known Legendre polynomial of order 2 and k and l correspond to any of the relaxation interactions under consideration here. Finally, it may be noted that any contribution arising from the scalar relaxation mechanism, characterized by A, is also neglected as they are usually orders of magnitude smaller than the terms under consideration. In the case of

CSR × DD cross-correlation the angle θ is the angle subtended by the r_{He} with the normal to the methyl protons plane, coinciding with the methyl C_3 rotation axis, as indicated in Fig. 1b.

The treatment of the methyl group is formally equivalent to the description of a spin-$\frac{3}{2}$ nucleus with axially symmetric quadrupolar and CSA interactions. The explicit formulation of the relevant Redfield matrix elements (*37*) for the DD, CSA, and CSR interactions is given in the single element base with subscripts referring to the energy levels in Fig. 1 by

$$\begin{pmatrix} R_{1111} \\ R_{1122} \\ R_{1133} \\ R_{1144} \\ R_{2222} \\ R_{2233} \\ R_{2244} \\ R_{3333} \\ R_{4444} \end{pmatrix} = \begin{pmatrix} 0 & -1 & -1 & 0 & -\frac{6}{5} & 0 & 0 & \frac{2\sqrt{6}}{\sqrt{5}} & 0 \\ 0 & 1 & 0 & 0 & \frac{6}{5} & 0 & 0 & \frac{2\sqrt{6}}{\sqrt{5}} & 0 \\ 0 & 0 & 1 & 0 & 0 & 0 & 0 & 0 & 0 \\ 0 & 0 & 0 & 0 & 0 & 0 & 0 & 0 & 0 \\ 0 & -1 & -1 & 0 & -\frac{14}{5} & 0 & 0 & \frac{2\sqrt{6}}{\sqrt{5}} & 0 \\ 0 & 0 & 0 & 0 & \frac{8}{5} & 0 & 0 & 0 & 0 \\ 0 & 0 & 1 & 0 & 0 & 0 & 0 & 0 & 0 \\ 0 & -1 & -1 & 0 & -\frac{14}{5} & 0 & 0 & \frac{2\sqrt{6}}{\sqrt{5}} & 0 \\ 0 & 1 & 0 & 0 & \frac{6}{5} & 0 & 0 & -\frac{2\sqrt{6}}{\sqrt{5}} & 0 \\ 0 & -1 & -1 & 0 & -\frac{6}{5} & 0 & 0 & \frac{2\sqrt{6}}{\sqrt{5}} & 0 \end{pmatrix} \times \begin{pmatrix} J_{DD}(0) \\ J_{DD}(\omega) \\ J_{DD}(2\omega) \\ J_{CSA}(0) + J_{CSR}(0) \\ J_{CSA}(\omega) + J_{CSR}(\omega) \\ J_{CSA}(2\omega) + J_{CSR}(2\omega) \\ J_{CSA\times DD}(0) + J_{CSR\times DD}(0) \\ J_{CSA\times DD}(\omega) + J_{CSR\times DD}(\omega) \\ J_{CSA\times DD}(2\omega) + J_{CSR\times DD}(2\omega) \end{pmatrix} \quad [13]$$

$$\begin{pmatrix} R_{1212} \\ R_{1223} \\ R_{1234} \\ R_{2323} \\ R_{2334} \\ R_{3434} \end{pmatrix} = \begin{pmatrix} -1 & -1 & -1 & -\frac{8}{15} & -2 & 0 & -\frac{4\sqrt{2}}{\sqrt{5}} & -\frac{2\sqrt{2}}{\sqrt{5}} & 0 \\ 0 & 0 & 0 & 0 & \frac{4\sqrt{3}}{\sqrt{5}} & 0 & 0 & \frac{2\sqrt{2}}{\sqrt{5}} & 0 \\ 0 & 0 & 1 & 0 & 0 & 0 & 0 & 0 & 0 \\ -1 & -1 & -1 & -\frac{8}{15} & -\frac{14}{15} & 0 & 0 & 0 & 0 \\ 0 & 0 & 0 & 0 & \frac{4\sqrt{3}}{\sqrt{5}} & 0 & 0 & -\frac{2\sqrt{2}}{\sqrt{5}} & 0 \\ -1 & -1 & -1 & -\frac{8}{15} & 0 & 0 & -\frac{4\sqrt{2}}{\sqrt{5}} & \frac{2\sqrt{6}}{\sqrt{5}} & 0 \end{pmatrix} \times \begin{pmatrix} J_{DD}(0) \\ J_{DD}(\omega) \\ J_{DD}(2\omega) \\ J_{CSA}(0) + J_{CSR}(0) \\ J_{CSA}(\omega) + J_{CSR}(\omega) \\ J_{CSA}(2\omega) + J_{CSR}(2\omega) \\ J_{CSA\times DD}(0) + J_{CSR\times DD}(0) \\ J_{CSA\times DD}(\omega) + J_{CSR\times DD}(\omega) \\ J_{CSA\times DD}(2\omega) + J_{CSR\times DD}(2\omega) \end{pmatrix}. \quad [14]$$

3. RESULTS

3.1. Simulations

For experimental comparison transfer functions are well suited. They describe the time evolution and interconversion of populations and coherences given by

$$T_{lp} \xrightarrow{\hat{R}t} \sum_{l' \geq |p|} f_{l'l}^{(p)}(t) T_{l'p}, \quad [15]$$

where $\hat{R}$ is the relaxation superoperator, $T_{l\rho}$ are the tensor operators, and the indices l and p are the rank and the coherence order of the tensor, respectively. The matrix elements $R_{ll'}^{(p)}$ of the relaxation superoperator, $\hat{R}$, which are eventually used in the simulations of the time evolution of transfer functions are obtained in the spherical tensor base by the employment of the transformation matrices $U^{(p)}$ given for each of the coherence $p = 0, \pm 1, \pm 2$ outlined in Refs. (*29, 30*).

The tensor operator of the form T_{l0} corresponds to Zeeman polarization for $l = 1$, and longitudinal two- and three-spin order respectively, for $l = 2$ and $l = 3$. A transfer function of the form $f_{l'l}^{(p)}(t)$ indicates the generation of p-quantum coherence of rank l' from p-quantum coherence of rank l.

Defining $R_n^{(p)}$ as eigenvalues of each of the subblock of the Redfield matrix, $\hat{R}^{(p)}$, and $a_{nl'l}$ as elements of the matrix M formed of eigenvectors of $\hat{R}^{(p)}$ given by

$$a_{nl'l} = \langle l'|M|n\rangle\langle n|M^{-1}|l\rangle, \quad [16]$$

one can write the transfer functions $f_{l'l}^{(p)}(t)$ as a linear combination of exponential functions as given below:

$$f_{l'l}^{(p)}(t) = \sum_n a_{nl'l} e^{R_n^{(p)} t}. \quad [17]$$

Since we will be dealing exclusively with transverse relaxation phenomena here, the generation of second- and third-rank single-quantum coherences from first-rank transverse magnetization is of prime interest. This time evolution can be represented as

$$T_{1,\pm1} \rightarrow f_{11}^{(\pm1)}(t) T_{1,\pm1} + f_{21}^{(\pm1)}(t) T_{2,\pm1} + f_{31}^{(\pm1)}(t) T_{3,\pm1}. \quad [18]$$

$T_{2,\pm1}$ is transverse two-spin order, and $T_{3,\pm1}$ is transverse three-spin order. In the vicinity of a paramagnetic center more two-spin order than three-spin order is generated. This is due to the greater significance of CSR × DD cross-correlation terms compared to DD × DD cross-terms, the latter prevailing in diamagnetic proteins (*28*) and for residues that are at a large distance (>12 Å) from the paramagnetic center in a paramagnetic protein.

Figure 2a shows the transfer functions $f_{11}^{(1)}(t)$, $f_{21}^{(1)}(t)$, and $f_{31}^{(1)}(t)$ assuming an electron-nuclear distance of 7 Å and an angle

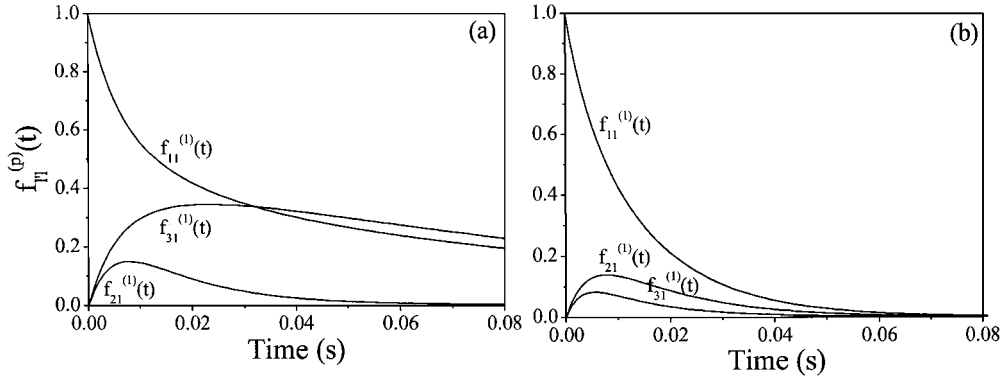

FIG. 2. A plot of the transfer functions, $f_{11}^{(1)}(t)$, $f_{21}^{(1)}(t)$, and $-f_{31}^{(1)}(t)$, as a function of the relaxation time with (a) no leakage terms and (b) with the addition of random field terms amounting to 20% of the magnitude of the diagonal elements of the Redfield density matrix. The leakage terms have a predominant effect on $f_{11}^{(1)}(t)$ and $f_{31}^{(1)}(t)$ and a minimal effect on $f_{21}^{(1)}(t)$, pointing to the dominance of CSR × DD cross-correlation terms as against CSA × DD terms in a paramagnetic protein. For the simulation the electron-nuclear distance, r_{He}, was assumed to be 7 Å, the angle θ (Fig. 1) to be 0°, the magnetic field, B_0, to be 11.74 T, and the correlation time τ_c to be 5 ns. A CSA of $\Delta\sigma_H = 10$ ppm was assumed.

of 0° for a correlation time of 25 ns. Figure 2b shows the same plots with random field terms added to the diagonal elements of the Redfield relaxation matrix. The measure of random field terms added amount to 20% of the diagonal elements of the Redfield relaxation matrix. This also shows that any random field terms influence more the DD × DD cross-terms than the CSR × DD cross-terms. From this plot it becomes clear that for a paramagnetic sample, $f_{21}^{(1)}(t)$ dominates over other transfer functions as it peaks faster. This establishes the fact that two-spin order should be more prominent in such systems than three-spin order which dominates in diamagnetic systems (*30*). For the parameters selected, maximum of $f_{21}^{(1)}(t)$ occurs around 5 ms. Figure 3 shows the maximum amplitude of $f_{21}^{(1)}(t)$ plotted as a function of the electron-nuclear distance, for a fixed correlation time of 5 ns and θ of 0°. This curve approaches the limiting curve of the CSA × DD case beyond a distance of approximately 12 Å. Figure 3 also shows the maximum of $f_{31}^{(1)}(t)$ plotted as a function of the electron-nuclear distance, for a fixed correlation time of 5 ns and θ of 0°. The two curves of $f_{31}^{(1)}(t)$ have been calculated with and without random field terms as indicated in the figure. The presence of a sizable DD × DD cross-correlation term that leads to a three-spin order which can be coverted to triplequantum coherence is evident from these curves. Hence the practically viable range for exploiting the cross-correlation effects, for an electronic spin $S_e = \frac{1}{2}$ case, is between 4 and 10 Å.

Figure 4 shows the angular dependence of $f_{21}^{(1)}(t)$ for a fixed electron-nuclear distance of 7 Å with other parameters remaining the same. The horizontal line shows the contribution of the CSA × DD cross-term which is not angular dependent for the bond geometry under consideration. From this figure it is evident that around the magic angle, 54.7°, the only contribution to

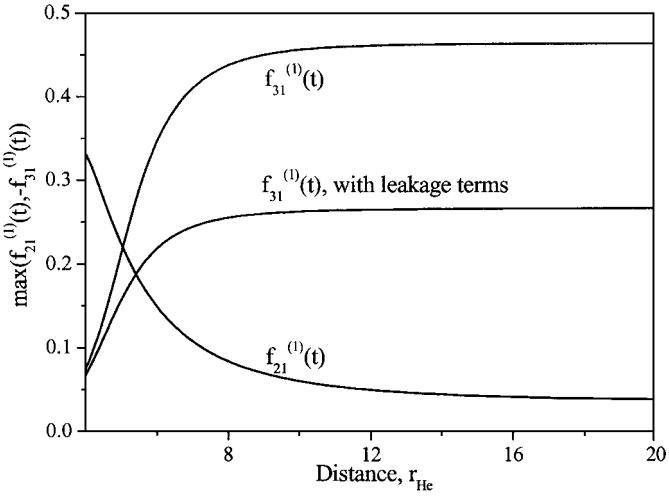

FIG. 3. A plot of the maximum value of the transfer function, $f_{21}^{(1)}(t)$ and $-f_{31}^{(1)}(t)$, as a function of the electron-nuclear distance (r_{He}) with the other simulation parameters being the same as in Fig. 2. The amount of leakage term corresponds to the same value as in Fig. 2.

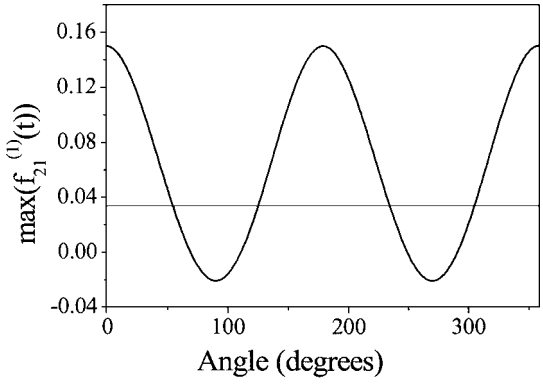

FIG. 4. A plot of the maximum value of the transfer function, $f_{21}^{(1)}(t)$, as a function of the angle, θ, with the other simulation parameters being the same as in Fig. 2, showing the full response with both CSR × DD and CSA × DD cross-correlation terms taken into account. The flat line shows the effect of the CSA × DD cross-term that acts as an offset to the CSR × DD cross-term.

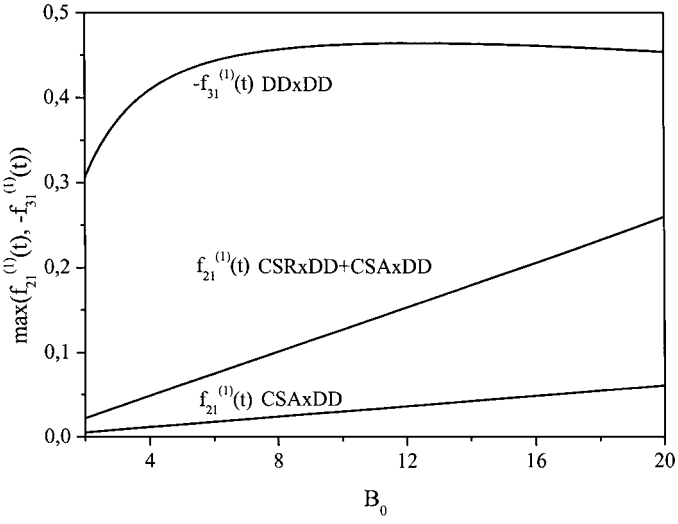

FIG. 5. A plot of the maximum value of the transfer functions, $f_{21}^{(1)}(t)$ and $-f_{31}^{(1)}(t)$, as a function of the magnetic field, B_0, with the other simulation parameters being the same as in Fig. 2. The response of the transfer function for both paramagnetic and diamagnetic proteins is shown in the figure.

$f_{21}^{(1)}(t)$ comes from the CSA × DD cross-terms as expected, while in all other angular regions, cross-terms involving CSR dominate. This makes the CSR × DD cross-correlation term a particularly strong and viable tool for arriving at geometric constraints in paramagnetic systems. In Fig. 5 the maximum of $f_{21}^{(1)}(t)$ is plotted as a function of the magnetic field and the importance of CSR above a field strength of approximately 10 T may be ascertained from the figure. The predominance of $f_{31}^{(1)}(t)$, meaning the prevalence of the DD × DD cross-term, can also be seen from the figure, where the maximum of $-f_{31}^{(1)}(t)$ is plotted as a function of the magnetic field. It is highly important for application on state-of-the-art and future spectrometers to compare the strengths of the cross-correlations as a function of the magnetic field. Figure 6a shows a plot of the spectral densities, $J(2\omega)$, $J(\omega)$, and $J(0)$, for each of the above cross-terms as a function of B_0. It is very clear that CSR × DD predominates over CSA × DD cross-terms. Figure 6b shows the $J(2\omega)$, $J(\omega)$, and $J(0)$ plot for each of the relaxation mechanisms, namely, DD, CSA, and CSR, as a function of B_0. Figure 6 shows the dominance of $J(0)$ spectral density at higher fields. Figure 6b underscores also a previously mentioned aspect of CSR relaxation: it affects transverse relaxation more than longitudinal relaxation.

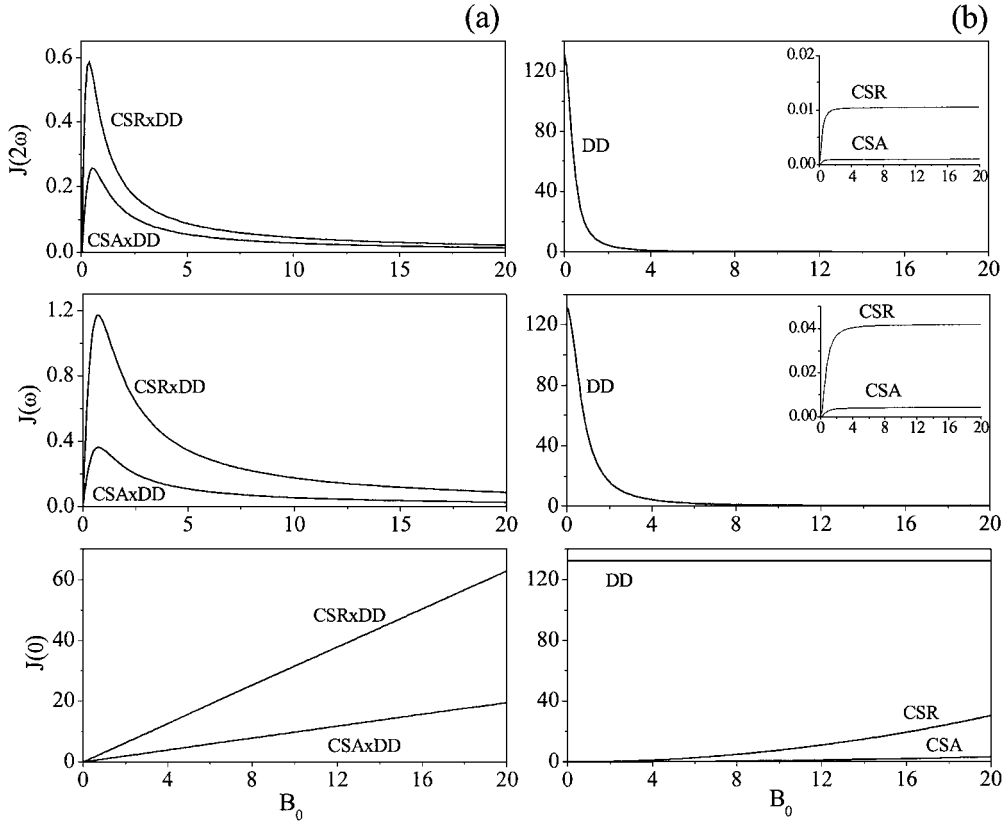

FIG. 6. (a) A plot of the spectral densities, $J(2\omega)$, $J(\omega)$, and $J(0)$, for both CSR × DD and CSA × DD cross-correlation terms as a function of the magnetic field, B_0, with the other simulation parameters being the same as in Fig. 2. (b) A plot of the spectral densities, $J(2\omega)$, $J(\omega)$, and $J(0)$, for DD, CSA, and CSR relaxation mechanisms as a function of the magnetic field. The behavior and magnitude of $J(0)$ over the other spectral densities clearly indicate the fact that the CSR cross-terms affect the transverse relaxation, T_2, times more than the longitudinal relaxation, T_1, times.

To make an order of magnitude estimate of how CSR influences both longitudinal and transverse relaxation mechanisms we examine the contribution to $J(0)$ in the case of transverse relaxation and $J(\omega)$ for longitudinal relaxation. Denoting by J_χ the spectral density associated with the CSR mechanism and J_S with the hyperfine or S contribution, the following expressions hold good:

$$
\begin{aligned}
J_\chi(0) &\sim 10^{-14}\left[\frac{g\beta B_0 S_e(S_e+1)\gamma_p\gamma_e\hbar}{3k_BT}\right]^2\frac{\tau_c}{r_{He}^6}\\
J_S(0) &\sim 10^{-14}(g\beta\gamma_p)^2 S_e(S_e+1)\frac{1}{r_{He}^6}\tau_e\\
J_\chi(\omega) &\sim J_\chi(0)\left(\frac{1}{1+\omega^2\tau_c^2}\right)\\
J_S(\omega) &\sim J_S(0)\left(\frac{1}{1+\omega^2\tau_e^2}\right)\\
\frac{J_\chi(0)}{J_S(0)} &\sim \frac{B_0^2 S_e(S_e+1)\gamma_e^2\hbar^2}{(k_BT)^2}\frac{\tau_c}{\tau_e}.
\end{aligned}
\qquad [19]
$$

Assuming the following values in SI units for the constants, $B_0 = 11.74$ T, $S_e = \frac{1}{2}$, $\tau_c = 10^{-9}$ s, and $\tau_e = 10^{-11}$ s, it may be seen that the contribution of CSR to transverse and longitudinal relaxation exceeds that of the contact term at least by an order of magnitude. This order of magnitude estimation assumes that the paramagnetic samples under investigation have a fast electron self-relaxation time constant, at least of the order of femto seconds, while the rotational correlation time has been assumed to be of the order of nano seconds.

Figure 7 shows the time evolution of $f_{21}^{(1)}(t)$ plotted at a high field of 20 T without assuming the presence of CSR and the same at 12 T with CSR present. In a paramagnetic system, the presence of additional cross-correlations creates rank 2 tensor terms at lower magnetic fields than in the case of diamagnetic systems where only cross-terms involving CSA can be exploited. This has a direct bearing on the recently introduced experiment, transverse relaxation-optimized spectroscopy, TROSY (*41*), which has been addressed already (*42*). The CSR part of the paramagnetic relaxation in the methyl group can hence be used as a viable probe for refining the structure of paramagnetic samples.

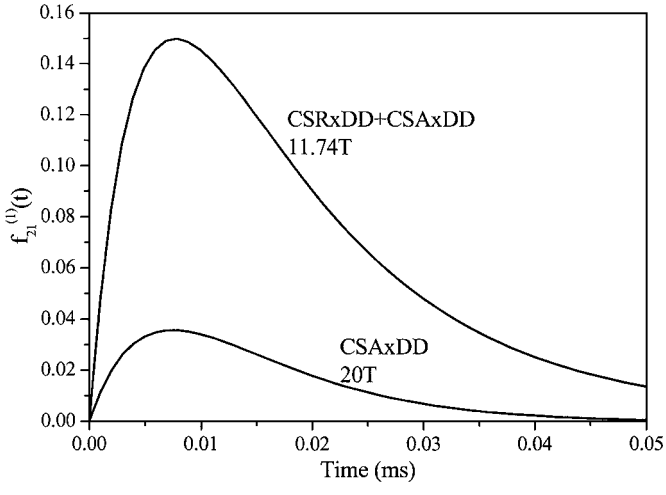

FIG. 7. A plot of the transfer function, $f_{21}^{(1)}(t)$, for a paramagnetic protein at 11.74 T and that for a diamagnetic protein at 20 T, as a function of the relaxation time, with the other simulation parameters being the same as in Fig. 2.

3.2. Experiments

Experiments were done on a sample of cyano-met-myoglobin, where Fe^{3+} is in the low spin ($S_e = \frac{1}{2}$) state. The low spin Fe^{3+}($S_e = \frac{1}{2}$) cyanide complex of myoglobin was prepared by adding excess KCN to the protein solution. The pH of the protein sample was adjusted to be at 6.0 using DCl. All NMR experiments were performed at 30°C on a Bruker Avance DRX-500 MHz spectrometer equipped with a triple-gradient triple-resonance inverse detection probe. Solvent signal presaturation was employed for suppression of residual water signals in all the experiments. A series of double-quantum (2Q)-filtered experiments was performed to determine the transfer functions using the pulse sequence indicated in Fig. 8a. In myoglobin the time evolution of two methyl groups, namely, Ile-99 γCH_3 (M1) and Ile-99 δCH_3 (M2) is monitored, the NMR assignments of which are known from previous work (*43*) which give ^1H signals that are well separated from others at -3.2 and -3.6 ppm. From the crystal structure, the r_{He} and θ of M1 and M2 are 7.13 Å, 35.7° and 6.8 Å, 72.59°, respectively. A number of 2Q-filtered T_2 experiments with different relaxation delays were carried out in the above sample, and the intensities of the resolved signal of the respective methyl groups are plotted as a function of the relaxation time, which corresponds to the delay, τ, in Fig. 8, represented by circles. The corresponding transfer function $f_{21}^{\pm1}(t)$ is plotted with the known distance and angle and shown as the continuous line. A good agreement between the experimental and theoretical curve is evident. This suggests that transfer functions are true representatives of the experimental parameters and a careful scrutiny of them will lead to geometrical constraints. The figure also shows double-exponential fits to the experimental curves, the fit taking the expression

$$I(t) = C(\exp(-\lambda_1 t) - \exp(-\lambda_2 t)), \qquad [20]$$

where $I(t)$ is the intensity of the 2Q signal as a function of the relaxation time, t, and λ_1 and λ_2 are the inverse time constants. It may be noticed from Eq. [13] that in principle the evolution of the transfer function, $f_{21}^{\pm1}(t)$, which is a measure of $I(t)$ is a triple exponential which in practice can be approximated by a double exponential. The transfer function $f_{21}^{\pm1}(t)$ has the general expression

$$f_{21}^{\pm1}(t) = a_{121}\exp(-\lambda_1 t) + a_{221}\exp(-\lambda_2 t) + a_{321}\exp(-\lambda_3 t). \qquad [21]$$

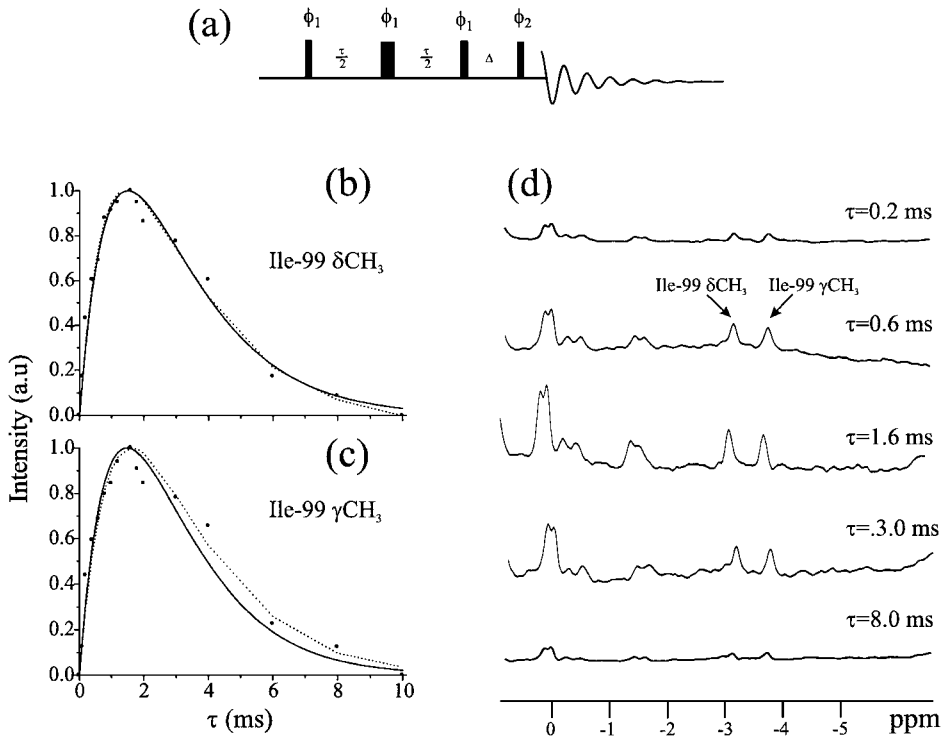

FIG. 8. (a) The pulse sequence used for the 2Q-filtered experiments where τ is the relaxation delay and Δ is the multiple-quantum filter delay. ϕ_1 is cycled so as to select, 2Q coherences and ϕ_2 is kept 90° out of phase with respect to ϕ_1 so as to preclude any 2Q coherence arising due to the scalar coupling. (b) A plot of the intensity of the double-quantum peaks corresponding to Ile-99 δCH_3 and (c) Ile-99 γCH_3 as a function of the relaxation time, given by the filled circles. The continuous line in (b) corresponds to a plot of the transfer function $f_{21}^{(1)}(t)$ with $r_{He} = 7.13$ Å and $\theta = 35.7°$ which is the geometry of Ile-99 γCH_3 and (c) corresponds to the transfer function $f_{21}^{(1)}(t)$ with $r_{He} = 6.8$ Å and $\theta = 72.59°$ which is the geometry of Ile-99 γCH_3. Also shown as a dotted line is the double-exponential fit to the experimental curves, the details of which are explained in the text. (d) One-dimensional 2Q-filtered spectra for a few τ delays indicated in the figure; 960 transients with a recycle delay of 1.5 s were accumulated for each of the experiments.

Table 1 gives the values of the exponents (λ's) from both simulation, assuming the known geometry parameters, and from a double-exponential fit to the plot of the experimental intensities of the two methyl groups corresponding to M1 and M2. It may be noted that the fitting of the coefficients is arbitrary, since for a biexponential function they must be equal in magnitude and opposite in sign, and the overall amplitude depends on other factors like the splitting of the resonance lines. The *a* coefficients are hence not listed in the table.

The good correspondence between the theoretical eigenvalues in the transfer function and those obtained from the fit can be seen from Table 1 with the time constants being a measure of both distance and angular constraints. It is worthwhile here to emphasize the fact that with a ^{13}C-labeled protein, individual T_2 measurements can be made from which the r_{He} can be measured, which then means that the methyl curves can be fitted unequivocally and unambiguously to the angle, thereby greatly simplifying the analysis.

TABLE 1
Coefficients and Exponents of $f_{21}^{(1)}(t)$ Obtained from a Double-Exponential Fit and Simulations

Methyl groups	λ_1	λ_2	λ_3
M1, theoretical	−837.55	−513.33	−13.50
M1, experimental	−835.80 ± 2.65	−507.00 ± 1.54	
M2, theoretical	−695.53	−549.80	−17.00
M2, experimental	−690.23 ± 2.66	−544.35 ± 2.10	

Employing initial rate approximation and Taylor expansion one can derive from Eq. [13] the following

$$\frac{df_{21}^{(1)}(t)}{dt} = \lambda_2 - \lambda_1, \qquad [22]$$

where λ_1 and λ_2 are the eigenvalues of Eq. [13] having nonzero coefficients. From Eq. [14] we see

$$\lambda_2 - \lambda_1 = \frac{4\sqrt{2}}{5}[J_{CSA\times DD}(0) + J_{CSR\times DD}(0)] \propto \frac{1}{r^3} P_2 \cos(\theta) \qquad [23]$$

with the proportionality condition holding good for $r < 15$ Å. Here we assume that the CSA of protons, $\Delta\sigma_H$, is of the order of 10 ppm. With this condition the above expression means that the slope of the initial part of the experimental curve is dependent

on $P_2\cos(\theta)/r^3$ although it has an offset term that depends on the weak contribution from the CSA × DD cross-correlation term (*30*).

4. CONCLUSIONS

The source of characteristic signatures of cross-correlation terms involving CSR in the relaxation behavior of the methyl protons in a paramagnetic protein, which were first reported in a previous publication (*28*), has been theoretically outlined here. The time evolution of the experimental amplitudes of methyl group signals corresponding to transverse two-spin order generated by the CSR × DD cross-correlation term correlate well with the theoretical transfer function derived from the known distance and angles from the x-ray structure of myoglobin. We propose to use this physical phenomenon to derive geometry constraints for three-dimensional structure refinements. Since from independent transverse relaxation time measurements distance constraints can be obtained, a single time-constant fit to such relaxation curves gives a direct measure of the angle. Experiments of this kind can thus lead to novel types of geometry constraints. To avoid overlap problems it will be necessary to use ^{13}C-labeled samples to disperse the peaks in a multidimensional experiment. Methyl groups are particularly abundant in the hydrophobic cores of proteins. Therefore geometry restriction based on methyl axis orientation can be valuable information augmenting other geometry constraints provided by either "classical" NOE-based techniques or more recent experiments (*18, 42*) based on CSR × DD cross-correlation in NH groups. In particular, combining the information on the orientation of the NH bond with that on the CH_3-axis orientation in alanine residues leads to restrictions for the ϕ-angle and thus can help in secondary structure discrimination. We expect that such kind of information will further enhance the study of paramagnetic biomolecules.

ACKNOWLEDGMENTS

This work was supported by the Austrian Science Foundation (FWF) through Project P12696 CHE and a Lise Meitner fellowship for P. K. Madhu (M531-CHE, M584-CHE).

REFERENCES

1. H. Shimizu, Theory of the dependence of nuclear magnetic relaxation on the absolute sign of spin–spin coupling constant, *J. Chem. Phys.* **40,** 3357–3364 (1964).
2. J. S. Blicharski, Interference effect in nuclear magnetic relaxation. II, *Phys. Lett. A* **24,** 608–610 (1967).
3. J. S. Blicharski, Interference effect in nuclear magnetic relaxation. III, *Acta Phys. Polon.* **38,** 19–24 (1970).
4. C. Dalvit and G. Bodenhausen, Measurement of dipole–dipole cross-correlation by triple-quantum filtered two-dimensional exchange spectroscopy, *Adv. Magn. Reson.* **14,** 1–33 (1990).
5. T. E. Bull, Relaxation in the rotating frame in liquids, *Prog. NMR Spectrosc.* **24,** 377–410 (1992).
6. L. G. Werbelow *in* "Nuclear Magnetic Resonance Probes of Molecular Dynamics" (R. Tycho, Ed.), p. 223, Kluwer Academic, Dordrecht/Norwell, MA (1994).
7. Anil Kumar, R. C. R. Grace, and P. K. Madhu, Cross-correlations in NMR, *Prog. NMR Spectrosc.* **37,** 191–319 (2000).
8. M. M. Fuson and J. H. Prestegard, Intensity exchange pulses for the extraction of cross-correlation spectral densites from coupled ^{13}C spectra of macromolecular systems, *J. Magn. Reson.* **41,** 179–184 (1980).
9. C. Dalvit and G. Bodenhausen, Proton chemical shift anisotropy: Detection of cross-correlation with dipole–dipole interactions by double quantum filtered two-dimensional NMR exchange spectroscopy, *Chem. Phys. Lett.* **161,** 554–560 (1989).
10. C. Dalvit and G. Bodenhausen, Evidence for dipolar cross-correlation from triple-quantum filtered two-dimensional exchange NMR spectroscopy, *J. Am. Chem. Soc.* **110,** 7924–7926 (1988).
11. P. S. Hubbard, Nonexponential relaxation of three-spin systems in nonspherical molecules, *J. Chem. Phys.* **51,** 1647–1651 (1969).
12. C. Maclean and E. L. Mackor, Transverse relaxation in systems of two nonidentical spins, *J. Chem. Phys.* **44,** 2708–2715 (1966).
13. R. C. R. Grace and Anil Kumar, Observation of cross-correlations in a weakly coupled ^{19}F–^{1}H four spin system, *J. Magn. Reson. A* **115,** 87–93 (1995).
14. M. Gueron, Nuclear relaxation in macromolecules by paramagnetic ions: A novel mechanism, *J. Magn. Reson.* **19,** 58–66 (1975).
15. A. J. Vega and D. Fiat, Nuclear relaxation processes of paramagnetic complexes. The slow motion case, *Mol. Phys.* **31,** 347–355 (1976).
16. I. Bertini, C. Luchinat, and D. Tarchi, Are true scalar proton–proton connectivities ever measured in COSY spectra of paramagnetic macromolecules? *Chem. Phys. Lett.* **203,** 445–449 (1993).
17. J. Qin, F. Delaglio, G. N. La Mar, and A. Bax, Distinguishing the effects of cross correlation and *J* coupling in COSY spectra of paramagnetic protein, *J. Magn. Reson.* **102,** 332–336 (1993).
18. J. Boisbouvier, P. Gans, M. Blackledge, B. Brutscher, and D. Marion, Long-range structural information in NMR studies of paramagnetic molecules from electron spin-nuclear spin cross-correlated relaxation, *J. Am. Chem. Soc.* **121,** 7700–7701 (1999).
19. R. Ghose and J. H. Prestegard, Electron spin-nuclear spin cross-correlation effects on multiplet splittings in paramagnetic proteins, *J. Magn. Reson.* **128,** 138–143 (1997).
20. I. Solomon, Relaxation processes in a two spin system, *Phys. Rev.* **99,** 559–565 (1955).
21. I. Solomon and N. Bloembergen, Nuclear magnetic interactions in the HF molecule, *J. Chem. Phys.* **25,** 261–266 (1956).
22. I. Bertini, C. Luchinat, M. Piccioli, and D. Tarchi, COSY spectra of paramagnetic macromolecules, observability, scalar effects, cross correlation effects, relaxation allowed coherence transfer, *Conc. Magn. Reson.* **6,** 307–335 (1994).
23. L. Mäler, F. A. A. Mulder, and J. Kowalewski, Paramagnetic cross-correlation effects in the longitudinal proton relaxation of *cis*-chloroacrylic acid in the presence of nickel(II) ions, *J. Magn. Reson. A* **117,** 220–227 (1995).
24. H. Desvaux and M. Gochin, Coherence transfer between nuclear spins in paramagnetic systems: Effects of nucleus–electron dipole–dipole cross-correlation, *Mol. Phys.* **96,** 1317–1333 (1999).
25. R. Brüschweiler, C. Griesinger, and R. R. Ernst, Correlated motion monitored by NMR relaxation in the rotating frame. A source of structural and

dynamic information on macromolecules, *J. Am. Chem. Soc*. **111,** 8034–8035 (1984).

26. R. Brüschweiler and R. R. Ernst, Molecular dynamics monitored by cross-correlated cross relaxation of spins quantized along orthogonal axes, *J. Chem. Phys*. **96,** 1758–1766 (1992).

27. B. Reif, M. Hennig, and C. Griesinger, Direct measurement of angles between bond vectors in high resolution NMR, *Science* **276,** 1230–1233 (1997).

28. P. K. Mandal, P. K. Madhu, and N. Müller, Nuclear magnetic relaxation of methyl protons in a paramagnetic protein—Cross-correlation effects, *Chem. Phys. Lett*. **320,** 269–276 (2000).

29. N. Müller, G. Bodenhausen, and R. R. Ernst, Relaxation-induced violations of coherence transfer selection rules in nuclear magnetic resonance, *J. Magn. Reson*. **75,** 297–334 (1987).

30. N. Müller and G. Bodenhausen, Cross correlation of chemical shift anisotropy and dipolar interactions in methyl proton investigated by selective nuclear magnetic resonance spectroscopy, *J. Chem. Phys*. **98,** 6062–6069 (1993).

31. A. Abragam, "Principles of Nuclear Magnetic Resonance," Clarendon, Oxford (1961).

32. I. Bertini and C. Luchinat, NMR of paramagnetic substances, *Coord. Chem. Rev*. **150** (1996).

33. H. Sternlicht, Nuclear relaxation induced by paramagnetic ions having anisotropic g factors, *J. Chem. Phys*. **42,** 2250–2251 (1965).

34. K. V. Vasavada and B. D. N. Rao, Nuclear spin relaxation in liquids due to interaction with paramagnetic ions having anisotropic g-tensors, *J. Magn. Reson*. **81,** 275–283 (1989).

35. I. Bertini, J. Kowalewski, C. Luchinat, and G. Parigi, Cross correlation between the dipole–dipole interaction and the Curie spin relaxation: The effect of anisotropic magnetic susceptibility, *J. Magn. Reson*. **152,** 103–108 (2001).

36. R. L. Vold and R. R. Vold, Nuclear magnetic relaxation in coupled spin systems, *Prog. NMR Spectrosc*. **12,** 79–133 (1978).

37. A. G. Redfield, Theory of nuclear relaxation processes, *Adv. Magn. Reson*. **1,** 1–19 (1965).

38. G. Esposito, A. M. Lesk, H. Molinari, A. Motta, N. Niccolai, and A. Pastore, Probing protein structure by solvent perturbation of nuclear magnetic resonance spectra, *J. Mol. Biol*, **224,** 659–670 (1992).

39. L. G. Werbelow and D. M. Grant, Intramolecular dipolar relaxation in multispin systems, *Adv. Magn. Reson*. **9,** 189–299 (1978).

40. L. G. Werbelow and D. M. Grant, Transverse relaxation of three identical spin-$\frac{1}{2}$ nuclei subject to shift anisotropy interactions, *J. Magn. Reson*. **20,** 554–564 (1975).

41. K. Pervushin, R. Riek, G. Wider, and K. Wüthrich, Attenuated T_2 relaxation by mutual cancellation of dipole–dipole coupling and chemical shift anisotropy indicates an avenue to NMR structures of very large biological macromolecules in solution, *Proc. Natl. Acal. Sci. USA* **94,** 12366–12371 (1997).

42. P. K. Madhu, R. Grandori, K. Hohenthanner, P. K. Mandal, and N. Müller, Geometry dependent two-dimensional heteronuclear multiplet effect in paramagnetic proteins, *J. Biomol. NMR* **20,** 31–37 (2001).

43. B. J. Hauksson, N. G. La Mar, K. R. Pandey, N. I. Rezzano, and M. K. Smith, ^{1}H NMR study of the role of individual heme propionates in modulating structural and dynamic properties of the heme pocket in myoglobin, *J. Am. Chem. Soc*. **112,** 6198–6205 (1990).